

1 This manuscript is a preprint and has not yet undergone peer-review. Hence, its final accepted version
2 may be different from the current one. Once the manuscript will be fully published the corresponding
3 DOI link will be added on the right-hand side of this webpage. Please, feel free to contact the
4 corresponding author if you have any feedback.
5

6 **Past and projected weather pattern persistence with associated multi-** 7 **hazards in the British Isles**

8

9 **Short title: Persistence of weather patterns over the British Isles**

10

11 Paolo De Luca^{1,2,3*}, Colin Harpham⁴, Robert L. Wilby¹, John K. Hillier¹, Christian L. E. Franzke⁵,
12 Gregor C. Leckebusch⁶

13

14 ¹Geography and Environment, School of Social Sciences, Loughborough University, Loughborough, UK

15 ²Department of Earth Sciences, Uppsala University, Uppsala, Sweden

16 ³Centre of Natural Hazards and Disaster Science (CNDS), Uppsala, Sweden

17 ⁴Climatic Research Unit (CRU), School of Environmental Sciences, University of East Anglia, Norwich, UK

18 ⁵Meteorological Institute and Center for Earth System Research and Sustainability (CEN), University of
19 Hamburg, Hamburg, Germany

20 ⁶School of Geography Earth and Environmental Sciences, University of Birmingham, Birmingham, UK

21

22 *Corresponding author

23 E-mail: p.deluca@lboro.ac.uk

24

25

26

27

28 **Abstract**

29 Hazards such as heatwaves and floods are often linked to persistent weather patterns. Atmosphere-
30 Ocean General Circulation Models (AOGCMs) are important tools for evaluating projected changes
31 in extreme weather. Here, we demonstrate that 2-day weather pattern persistence is a useful concept
32 for both investigating climate risks from multi-hazard events as well as for assessing AOGCM realism.
33 This study evaluates the ability of a Coupled Model Intercomparison Project Phase 5 (CMIP5) multi-
34 model sub-ensemble of 10 AOGCMs at reproducing seasonal weather pattern persistence and
35 frequencies over the British Isles. Changes in persistence are investigated under two Representative
36 Concentration Pathways (RCP8.5 and RCP4.5) up to 2100. Broadly, the ensemble replicates historical
37 weather type persistence observed in reanalyses (1971-2000). Future persistence and frequency of
38 summer anticyclonic patterns are found to increase, implying heightened risk of drought and
39 heatwaves. On the other hand, the cyclonic weather type decreases in autumn suggesting reduced
40 likelihood of flooding and severe gales. During winter, AOGCMs suggest increased risk of concurrent
41 flood-wind hazards by 2100, however, they also tend to over-estimate such risks when compared to
42 reanalyses. In summer, the strength of the nocturnal Urban Heat Island (UHI) of London is expected
43 to intensify, enhancing the likelihood of combined heatwave-poor air quality events. Further research
44 is needed to explore other multi-hazards in relation to changing weather pattern persistence and how
45 best to communicate such threats to vulnerable communities.

46

47

48

49

50

51

52 **1. Introduction**

53 Persistent weather patterns can translate into hazards such as heatwaves, poor air quality, drought,
54 wildfires and episodes of flooding [1–4], with significant socio-economic losses [5,6]. Examples of
55 such impactful episodes include the 2003 and 2010 European summer heatwaves that led to more than
56 100,000 deaths, reduced gross primary productivity of crops and, in the latter episode over Russia,
57 about US\$15 billion economic losses [7–10]. Similarly, summer 2013 in eastern China, was the hottest
58 ever recorded in that region, with persistent and widespread heatwaves and droughts causing severe
59 socio-economic impacts amounting to 59 billion RMB in losses [11]. Conversely, the extremely wet
60 and stormy 2013/14 winter over the United Kingdom (UK) was characterised by the passage of
61 numerous low-pressure systems causing extensive pluvial, fluvial, coastal and groundwater flooding
62 along with severe gales [12–14].

63
64 A growing body of literature is discussing possible dynamical mechanisms linking Arctic
65 Amplification (AA) [15] (the faster warming of the Arctic compared to the global scale) with more
66 persistent weather patterns across the northern hemisphere mid-latitudes [1–4,16,17]. The influence of
67 AA on the polar jet stream is the dynamical mechanism that has attracted most attention from the
68 media, policy makers and scientists. In fact, since AA began to be observed in the late 1980s, the jet
69 stream has assumed a wavier [2–4,18–20] and weaker [3,4,20,21] character, which accounts for more
70 persistent weather patterns, and hence impactful extreme events in the northern mid-latitudes
71 [16,17,22,23]. Meanwhile, analysis of weather type occurrence and persistence in historical and 21st
72 century climate model runs, under different Representative Concentration Pathways (RCPs), is
73 becoming relevant for assessing the dynamical realism of models as well for describing associated
74 weather and climate extremes [24–27]. By focusing on weather type persistence both model realism
75 and phenomena associated with the AA can be examined.

76

77 Natural hazards pose a significant socio-economic threat, yet their spatio-temporal co-occurrence
78 (termed herein *multi-hazards*) are not yet fully understood [28,29]. Multi-hazards/risks research has
79 grown considerably over the last decade [30–34], such that the United Nations Sendai Framework for
80 Disaster Risk Reduction (UNISDR) [35] has called for multi-hazard approaches to disaster risk
81 reduction. Examples of multi-hazard studies include interactions between earthquakes and landslides
82 [36], multi-basin flooding and extra-tropical cyclones [37], river and coastal flooding [38], extreme
83 wet and dry hydrological events [39].

84

85 Considering natural hazards as physical processes that can interact across both temporal and spatial
86 scales is of interest to decision makers such as governments, local businesses, emergency management
87 services and (re)-insurance companies. Until recently, natural hazards were almost always considered
88 as independent perils. However, since they can compound in various ways (i.e. occur simultaneously,
89 as cascades or cumulatively) over a sufficiently long time-frame [35], their combined socio-economic
90 impacts can exceed what was originally planned for, putting societies and economies under stress [28].

91

92 Previous studies have investigated linkages between weather patterns (or large-scale atmospheric
93 circulation) and local extreme events, such as heavy rainfall, storms, floods and heatwaves [27,37,40–
94 46]. The conventional approach to flood analysis at the *single* catchment scale is being extended to
95 frameworks with inter-related hazards, driven by global climate modes, covering *multiple* catchments
96 [41]. Others show that the bias in simulating regional extreme precipitation days by an Atmosphere-
97 Ocean General Circulation Model (AOGCM) is reduced by applying atmospheric circulation indices
98 [43]. Moreover, weather patterns extracted from AOGCMs have also been used to downscale local
99 climate variables, such as temperature, precipitation, radiation and humidity at local scales [27,47,48].
100 However, AOGCMs vary in their ability to simulate the frequency, seasonality and persistence of
101 weather patterns at regional scales [27,44]. Some studies have linked heavy precipitation events to

102 atmospheric circulation states, such as the 850hPa geopotential height field or integrated vapour
103 transport (IVT) [42], and found connections between selected weather patterns and multi-basin
104 flooding driven by extra-tropical cyclones (ETCs) [37]. Others have used weather patterns to quantify
105 changes in the strength of the nocturnal Urban Heat Island (UHI) – a phenomenon that may be
106 associated with combined heatwave and air pollution events within cities [40].

107

108 Previous evaluations for Europe and the British Isles (BI) show that Coupled Model Intercomparison
109 Project Phase 5 (CMIP5) AOGCMs generally reproduce synoptic-scale weather patterns, calculated
110 using daily sea-level pressure (SLP) fields, but there are recognized biases [49,50]. For example,
111 CMIP5 AOGCMs are not yet able to simulate correctly the number of anticyclonic (A-type) patterns
112 and hence blocking episodes, with the former being underestimated in northern Europe and the BI, but
113 overestimated in southern Europe [49–51]. Other biases are found for cyclonic (C-type) and westerly
114 (W-type) occurrences, with both being overestimated across Europe [49]. These studies also examined
115 future changes in frequency of weather patterns and blocking episodes by comparing historical
116 conditions with RCP8.5, to determine how such changes might affect European temperatures. The A-
117 type is projected to increase significantly over the BI during all seasons except for winter (DJF), the
118 C-type to decrease in all seasons, and the W-type to increase except in summer (JJA) by the end of the
119 century [49]. Overall, blocking episodes are projected to decrease for the BI in DJF and JJA by 2061-
120 2090 (RCP8.5) [51].

121

122 We extend these analyses by assessing the ability of a CMIP5 [52] multi-model sub-ensemble (MME)
123 of 10 AOGCMs at reproducing historical seasonal persistence of daily weather patterns, here identified
124 as Lamb Weather Types (LWTs) over the BI [53–56]. We define 2-day persistence as the probability
125 that a given LWT will occur on any two successive days. Climate model simulations of historic
126 weather patterns are compared with those derived from 20CR [57], NCEP [58] reanalyses, and Lamb’s

127 catalogue of subjectively defined weather types [53,59]. We investigate how persistence and seasonal
 128 frequencies are projected to change within the full 21st century under RCP8.5 and RCP4.5, with
 129 persistence assessed for both the MME mean (MME) and individual AOGCMs. We also quantify
 130 and discuss the implications of future multi-hazards, here identified as nearly concurrent multi-basin
 131 flooding and ETCs impacting Great Britain (GB) in winter [37] or combined summer heatwave and
 132 poor air quality events over London [40]. Thus, two multi-hazard metrics are applied, along with their
 133 evaluation under RCP8.5 and RCP4.5 projections up to 2100: likelihood of (1) multi-basin flooding
 134 (*F-Score*) and (2) changing intensity of the nocturnal *Urban Heat Island (UHI)*.

135

136

137 **2. Methods and Data**

138 **2.1 Lamb Weather Types (LWTs)**

139 Daily atmospheric sea-level pressure (SLP) patterns are categorized using the system of Lamb Weather
 140 Types (LWTs) [53] via an objective classification scheme centred over the BI (Fig 1) [54,56]. Choice
 141 of the LWTs objective scheme is justified by the fact that this methodology and weather typing
 142 classification was originally developed for the BI. LWTs of similar airflow properties are derived from
 143 a 5° by 10° latitude-longitude grid array (Fig 1) and computed from daily (12 UTC) SLP values at
 144 each grid point. The airflow characteristics are expressed by the following set of equations, where the
 145 integers in bold correspond to the grid point reference numbers in Fig 1:

146

$$147 \quad W = \frac{1}{2}(\mathbf{12} + \mathbf{13}) - \frac{1}{2}(\mathbf{4} + \mathbf{5}) \quad \text{(westerly flow)} \quad (1)$$

148

$$149 \quad S = 1.74 \left[\frac{1}{4}(\mathbf{5} + 2.0 \times \mathbf{9} + \mathbf{13}) - \frac{1}{4}(\mathbf{4} + 2.0 \times \mathbf{8} + \mathbf{12}) \right] \quad \text{(southerly flow)} \quad (2)$$

150

151 $F = (S^2 + W^2)^{1/2}$ (resultant flow) (3)

152

153 $ZW = 1.07 \left[\frac{1}{2}(\mathbf{15} + \mathbf{16}) - \frac{1}{2}(\mathbf{8} + \mathbf{9}) \right] - 0.95 \left[\frac{1}{2}(\mathbf{8} + \mathbf{9}) - \frac{1}{2}(\mathbf{1} + \mathbf{2}) \right]$
 154 (westerly shear vorticity) (4)

155

156 $ZS = 1.52 \left[\frac{1}{4}(\mathbf{6} + 2.0 \times \mathbf{10} + \mathbf{14}) - \frac{1}{4}(\mathbf{5} + 2.0 \times \mathbf{9} + \mathbf{13}) - \frac{1}{4}(\mathbf{4} + 2.0 \times \mathbf{8} + \mathbf{12}) \right]$
 $\quad \quad \quad + \frac{1}{4}(\mathbf{3} + 2.0 \times \mathbf{7} + \mathbf{11})$
 157 (southerly shear vorticity) (5)

158

159 $Z = ZW + ZS$ (total shear vorticity) (6)

160

161 Flow units are derived from the geostrophic approximation (each equivalent to 1.2 knots) and they are,
 162 along with the geostrophic vorticity units, expressed as hPa per 10° latitude at 55°N (100 units are
 163 equivalent to $0.55 \times 10^{-4} = 0.46$ times the Coriolis parameter at 55°N). Three coefficients are used within
 164 equations (2, 4 and 5) to account for variations in relative grid spacing at different latitudes with
 165 latitude (ψ) here set as 55° [56]: S is multiplied by 1.74, derived from $1/\cos(\psi)$; ZW , 1.07 and 0.95
 166 from $\sin(\psi)/\sin(\psi-5^\circ)$ and $\sin(\psi)/\sin(\psi+5^\circ)$; ZS , 1.52 from $1/2(\cos(\psi)^2)$.

167

168 The last step for defining LWTs is to apply five rules [53,54,56]:

169

170 i) the flow direction is given by $\tan^{-1}(W/S)$ and is calculated on an eight-point compass with 45° per
 171 sector. If W is positive, add 180°. Thus, the W -type occurs between 247.5° and 292.5°;

172

173 ii) Lamb pure directional weather types (e.g. N, S, or E-types) correspond to an essentially straight
 174 flow, when $|Z|$ is less than F ;

175

176 iii) Lamb's pure cyclonic (C) and anticyclonic (A) types are identified when $|Z|$ is greater than $2F$,
177 respectively with $Z > 0$ and $Z < 0$;

178

179 iv) Lamb's hybrid types (e.g. AE and CSW) are characterised by a flow partially anticyclonic/cyclonic,
180 with $|Z|$ lying between F and $2F$;

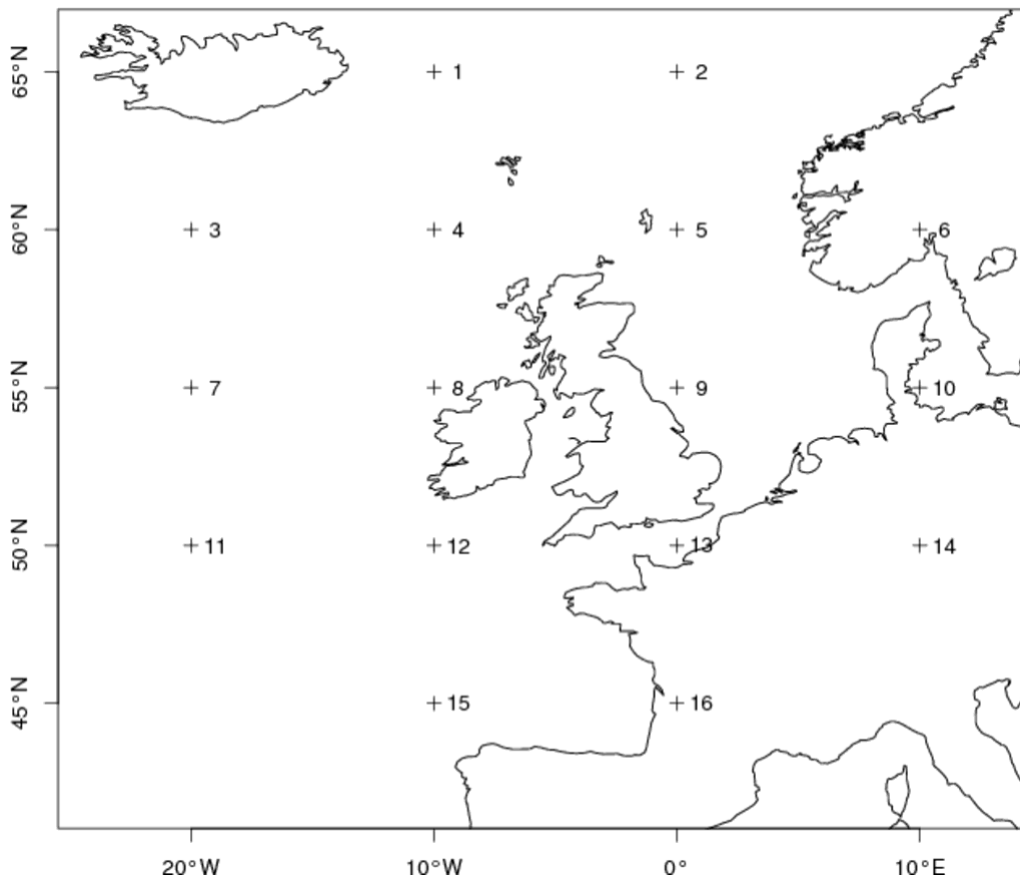
181

182 v) the unclassified (U) type is obtained when F and $|Z|$ are less than 6, with the choice of 6 depending
183 on grid spacing.

184

185 The objective classification scheme yields 27 LWTs comprised of two synoptic types (A and C), five
186 purely directional types (W, NW, E, N, and S) , 19 hybrid combinations of synoptic and directional
187 types (e.g. CNW, CSE and AE), and 1 unclassified (U) type [54,56]. For persistence and frequency
188 analyses, we focus on the 7 synoptic and directional LWTs plus the U-type; counts of hybrid types
189 were spread across the main types as per Lamb's original definition [53,60] and common practice
190 within earlier studies [54,55,61,62]. We assess LWT persistence and frequency for summer (June-
191 July-August, JJA), autumn (September-October-November, SON), winter (December-January-
192 February, DJF) and spring (March-April-May, MAM). On the other hand, when calculating indices of
193 future multi-hazards, the hybrid LWTs were not incorporated into the 7 main types as the F-Score and
194 nocturnal UHI indices require these weather patterns to be considered independently.

195



196

197 **Fig 1. Grid points used to calculate Jenkinson flow and vorticity terms for the British Isles (BI).** Numbers
 198 refer to those points used in Equations 1 to 5.

199

200

201 **2.2 Data**

202 Weather patterns were derived from the SLP produced by each AOGCM in our CMIP5 MME listed

203 in Table 1 [52]. We defined the historical period as the 1980s (1971-2000) whereas the future was

204 divided into three 30-year periods: the 2020s (2011-2040), 2050s (2041-2070) and 2080s (2071-2100).

205 The CMIP5 AOGCMs and MMEM outputs for the historical period was compared with LWTs derived
 206 from 20CR [57], NCEP [58] reanalyses and Lamb's subjective catalogue, which ends in 1997 [53,59].

207 The MMEM was built by first computing the LWTs and relative seasonal persistence and frequencies
 208 per each AOGCM then averaging these values within each time period.

209

210 **2.3 Persistence and trend analyses**

211 Weather pattern persistence is defined here as the conditional probability (p_{ij}) that a given LWT_j on
212 day(t) is followed by the same LWT_j on day($t+1$) [63,64]. This diagnostic was extracted for the 7 main
213 LWTs and the U-type using the diagonal cells of Markov-chain transition matrices. This enabled
214 estimation of historical (1980s) and future (2020s, 2050s and 2080s) seasonal persistence for the
215 MMEM as well as for individual AOGCMs for impactful weather types and seasons, the 20CR, NCEP
216 reanalyses and Lamb's subjective catalogue.

217

218 Uncertainty in p_{ij} for the 1980s was calculated by boot-strapping ($n=1,000$) 30-year seasonal
219 simulations using the *markovchain* package within the R framework [65]. This algorithm
220 stochastically generates n series of daily LWTs from the original conditional distributions of the
221 weather patterns in each AOGCM, then recomputes p_{ij} from each series. The resulting $p^{BOOTSTRAP}_{ij}$ is
222 the mean of all p_{ij} across the 1000 series, for each AOGCM. The 95% confidence intervals of
223 $p^{BOOTSTRAP}_{ij}$ are obtained from the cumulative distribution of the 1000 values of p_{ij} for each AOGCM.

224

225 Statistical significance of changes in persistence for the AOGCM sub-*ensemble* between the 1980s
226 and future periods (S1 and S2 Tables) was assessed using a Mann-Whitney-Wilcoxon two-tailed test
227 [66] applied to the 10 estimates of $p^{BOOTSTRAP}_{ij}$ for each time period. Changes in p_{ij} between the 1980s
228 and future periods for *individual* AOGCMs were regarded as statistically significant if future
229 persistence of a given LWT and AOGCM fell outside the 95% confidence intervals of the $p^{BOOTSTRAP}_{ij}$
230 range of that AOGCM for the 1980s (Fig 3 and S2 Fig).

231

232 To detect both linear and non-linear annual changes in the total seasonal counts of LWTs MMEM
233 frequencies under RCP8.5 and RCP4.5 scenarios, a trend analysis was performed for the 2006-2100
234 time period. For illustrative purposes, we only show trends for anticyclonic (A, summer JJA), cyclonic

235 (C, autumn SON) and westerly (W, winter DJF) types as indicators of impactful weather across the BI
 236 (Fig 4 and S3 Fig). Results are also presented for the southerly (S, spring MAM) types as this LWT
 237 shows most significant changes in seasonal persistence according to the non-parametric Mann-
 238 Whitney-Wilcoxon two-tailed test between the 1980s and each of the three future periods (i.e. 2020s,
 239 2050s and 2080s). A modified Mann-Kendall test, which takes into account possible autocorrelation
 240 within the time series, was applied to both RCP8.5 and RCP4.5 seasonal MMEM LWTs frequencies
 241 [67]. The significance of trends, along with their relative Sen's slopes, are shown in S3 Table [68].

242

243 **2.4 Indices of winter flood-wind hazards and summer UHI intensity**

244 As a measure of concurrent flood-wind hazards we calculated an extended version of the F-Index
 245 [37,69], here defined as the F-Score, for each single AOGCM, MMEM, NCEP, 20CR and Lamb's
 246 subjective datasets, covering the 1980s, 2020s, 2050s and 2080s, for selected LWTs known to drive
 247 these multi-hazard events [37] during winter under both RCP8.5 (Fig 5) and RCP4.5 (S4 Fig). The F-
 248 Index is the ratio of observed to expected frequency of floods for a given LWT, where values greater
 249 than 1 show higher than expected likelihood. Ten LWTs are known to be associated with historic,
 250 multi-basin floods [37], of which eight (C, CS, CSW, CNW, S, SW, W, and NW-types) increase their
 251 likelihood and two (N and A-types) reduce likelihood. All other LWTs are weighted zero. The F-Score
 252 is then calculated by multiplying the winter DJF frequencies ($freq_djf_j$) of these LWTs by their
 253 F_Index_j (as per Event Set E in [37]) and by summing these values:

254

$$255 \quad F_Score_i = \sum_{j=1}^{10} freq_djf_{j,i} \times F_Index_{j,i}$$

256 (7)

257

258 where i represents the single AOGCM, NCEP, 20CR and Lamb's subjective datasets within the
 259 relative time periods of 1980s, 2020s, 2050s, 2080s and j is the given LWT considered from the 10
 260 types mentioned above. The higher the F-Score, the greater the likelihood of concurrent multi-basin
 261 flood and wind hazards within winter, over the specified time horizon and RCP scenario.

262

263 As a proxy for combined heatwave and poor air quality hazards occurring during summer, we use
 264 observed, simulated and projected nocturnal UHI temperatures in tenths of degree Celsius for London
 265 (UK) [40], using the same datasets, time periods and RCPs as per the F-Score (Fig 6 and S5 Fig). The
 266 UHI phenomenon is caused by absorption and trapping of heat as well as by changed airflows and
 267 sensible heat fluxes within the built environment. The simplest form of UHI metric (used by [40]) is
 268 based on the daily temperature difference between an urban and rural reference site (during daylight
 269 or night hours). These values may then be stratified by LWT to show the extent to which some weather
 270 patterns favour extreme UHI episodes. The UHI metric was derived as follows by: i) multiplying LWT
 271 summer JJA frequencies ($freq_jja_h$) by their respective average UHI intensities taken from [40]
 272 (UHI_w_h); ii) summing these values; and iii) dividing the total from step ii) by the total number of
 273 days in the period analysed ($days_h$) to give the mean daily UHI intensity:

274

275

$$UHI_i = \sum_{h=1}^{27} \frac{freq_jja_{h,i} \times UHI_w_{h,i}}{days_{h,i}}$$

276

(8)

277

278 where i is the same notation as per the F-Score and h refers to the 27 LWTs.

279

280 To assess the statistical significance of changes between the AOGCMs 1980s and future 2020s, 2050s
 281 and 2080s periods, for both the F-Score and nocturnal UHI temperatures, we applied a similar approach

282 as per persistence. Here, $n=1,000$ boot-strapped samples of daily LWT series (based on conditional
283 distributions for all seasons combined) were generated for each AOGCM run in the 1980s. Next, the
284 F-Score or UHI were calculated for every series and AOGCM, then averaged and confidence limits
285 established as before. This procedure shows the extent to which estimates for the future indices fall
286 within the 95% confidence range of the boot-strapped estimate for each AOGCM in the 1980s.

287

288 Sample sizes varied depending on the index and AOGCM. For the F-Score, we considered the period
289 1971-2001 to capture January and February of winter 2000/01. Here, models with leap years have a
290 total of 11,323 days, models without leap years 11,315 days and the HadGEM2-ES model (with 360
291 days per year) has 11,160 days. For the UHI, the calendar years 1971-2000 were used as we are
292 interested in summer temperatures, with leap year AOGCMs having 10,958 days, non-leap years
293 models 10,950 days and the HadGEM2-ES 10,800 days.

294

295

296

297

298

299

300

301

302

303

304

305

306

307 **Table 1. CMIP5 multi-model sub-ensemble (MME) used in the analyses.**

Model name	Research institute	Lat-Lon resolution	Ensemble member
HadGEM2-ES	Met Office, United Kingdom	1.25° × 1.875°	r1i1p1
MPI-ESM-LR	Max Planck Institute for Meteorology, Germany	1.9° × 1.9°	r1i1p1
MRI-CGCM3	Meteorological Research Institute, Japan	1.1° × 1.1°	r1i1p1
CNRM-CM5	National Centre for Meteorological Research, France	1.4° × 1.4°	r1i1p1
CanESM2	Canadian Center for Climate Modeling and Analysis, Canada	2.8° × 2.8°	r1i1p1
MIROC5	Model for Interdisciplinary Research on Climate, Japan	1.4° × 1.4°	r1i1p1
CSIRO-Mk3.6.0	Commonwealth Scientific and Industrial Research Organisation, Australia	1.9° × 1.9°	r10i1p1
IPSL-CM5A-LR	Institute Pierre-Simon Laplace, France	1.9° × 3.75°	r1i1p1
CCSM4	National Center for Atmospheric Research, USA	0.94° × 1.25°	r6i1p1
GFDL-CM3	Geophysical Fluid Dynamics Laboratory, USA	2° × 2.5°	r1i1p1

308

309 The columns in Table 1 show the: (1) CMIP5 model name; (2) research institute where the model was
 310 developed; (3) resolution as latitude by longitude in degrees; and (4) ensemble member analysed. For all models
 311 the historical and RCP8.5 (and RCP4.5) sea-level pressure (SLP) outputs are used to calculate daily LWTs for
 312 the BI.

313

314

315

316 **3 Results**

317 **3.1 Persistence of weather patterns (MME)**

318 The A, C and W patterns are the most frequent weather types affecting the BI. Overall, the MME
319 replicates weather type persistence during the four climatological seasons when compared with 20CR
320 [57] and NCEP [58] reanalyses for the historical period (1980s) (Fig 2). There is less agreement
321 between Lamb's subjectively classified daily weather catalogue and both the MME and reanalyses. A-
322 type persistence is more variable within the MME and on average underestimated in winter, consistent
323 with previous studies [49,50]. There is closer agreement for the A-type in other seasons.

324

325 W-type persistence agrees with the reanalyses but is always less than in Lamb's catalogue. C-type
326 persistence is overestimated by the MME in all seasons when compared to reanalyses as reported
327 before [49] for Europe more generally. Such biases in the C-type could be interpreted as exaggerating
328 the likelihood of flooding in the MME compared with reanalyses [69].

329

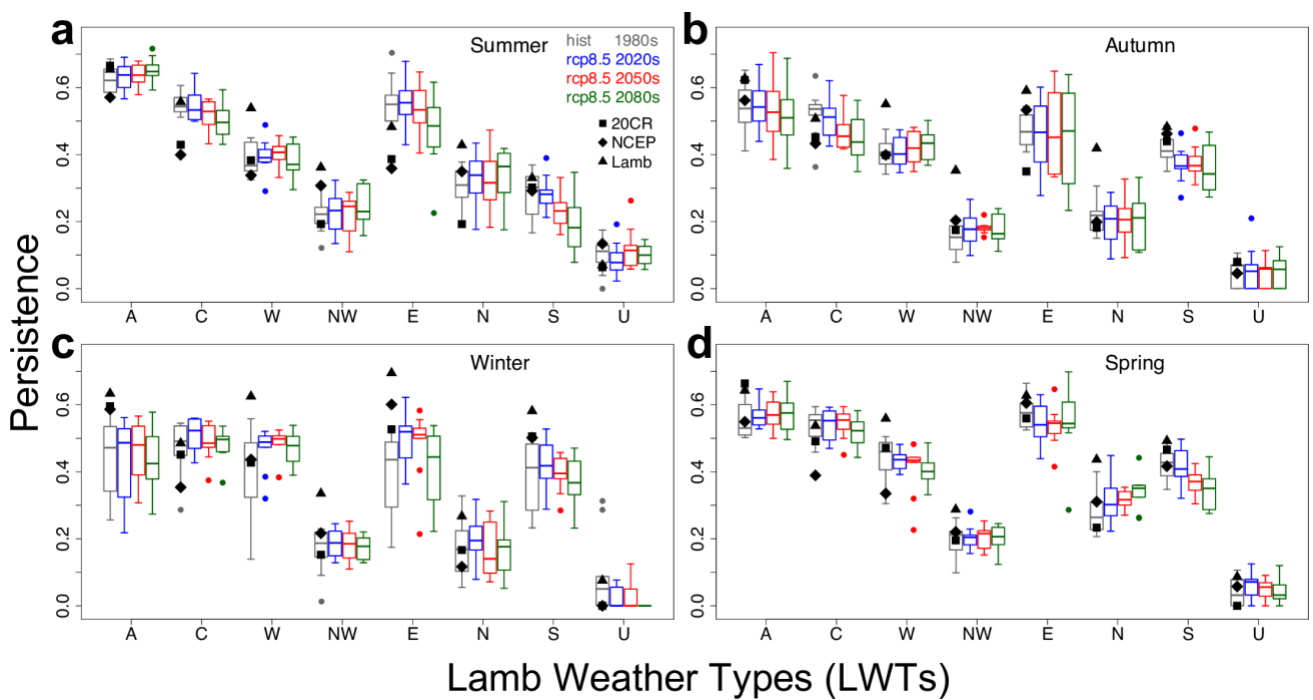
330 Fig 2 shows that the distributions of persistence are asymmetrical (or skewed) around the MME means
331 for many of the weather types and time periods. This characteristic suggests potentially large biases in
332 the estimation of extreme events, if studies rely on only single or a few AOGCMs. Changes in weather
333 type persistence between the ensembles of historical and future periods within RCP8.5 (Fig 2) are
334 weakly significant ($p\text{-value} < 0.1$, Mann-Whitney-Wilcoxon two-tailed test) for the C-type in summer
335 and autumn by 2080s; W-type in winter by 2050s; E-type in summer by 2080s and winter for the 2020s
336 and 2050s; N-type in spring by 2050s and 2080s; and S-type in summer by 2080s, autumn in all periods
337 and spring by 2050s and 2080s (S1 Table).

338

339 Results for RCP4.5 show similar changes in persistence compared to RCP8.5, although they are less
 340 substantial (S1 Fig). In particular, the C-type is found to change significantly ($p < 0.1$) only in summer
 341 by the 2080s; the E-type in winter by the 2080s; the N-type only in spring by the 2080s; and the S-
 342 type in summer by the 2050s and spring also by the 2020s (S2 Table).

343

344



345

346 **Fig 2. Persistence of the seven main LWTs plus unclassified (U) type under RCP8.5.** Persistence is
 347 calculated for (a) summer, (b) autumn, (c) winter and (d) spring, for the historical 1980s period (1971-2000)
 348 and under RCP8.5 by the 2020s (2011-2040), 2050s (2041-2070) and 2080s (2071-2100). Boxplots show
 349 distributions of persistence in each LWT, for the 10-member AOGCM ensemble, compared with 20CR, NCEP
 350 and the Lamb's catalogue. Segments show the minimum, 1st quartile, median, 3rd quartile and maximum.
 351 Outliers are shown by dots.

352

353

354 3.2 Persistence of weather patterns (by model)

355 Fig 3 shows persistence for the same future periods but for each AOGCM in the MME compared with
 356 the reanalyses and Lamb's catalogue, for impactful weather types and seasons. Significance of changes

357 was assessed against the boot-strapped confidence limits for the 1980s. Most model projections under
358 RCP8.5 fall outside the 95% confidence intervals of historical persistence. A-type MMEM persistence
359 increases during summer (Figs 2a and 3a); C-type persistence decreases in all seasons, most markedly
360 in summer and autumn (Figs 2 and 3b); W-type persistence does not change in winter but increases in
361 autumn and decreases in spring (Figs 2b-d and 3c).

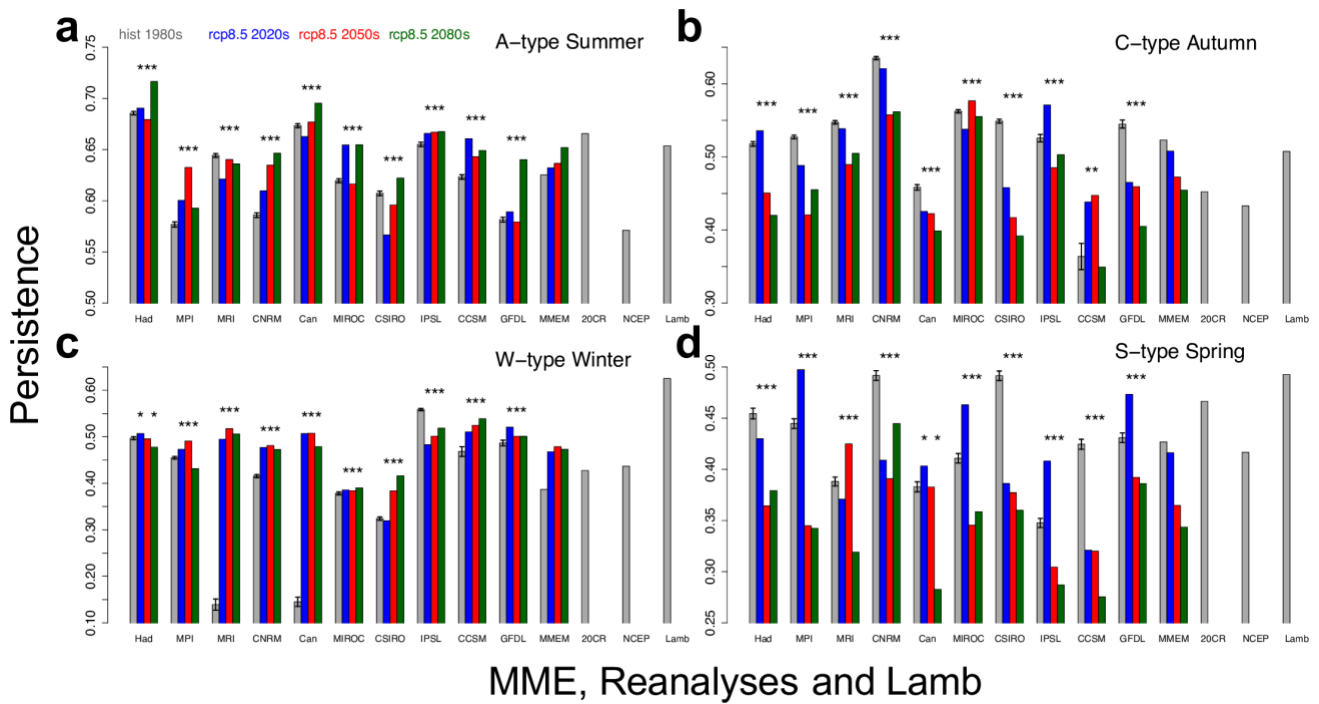
362

363 Amongst the other weather types, we note only a decrease in C- and E-types during summer, an
364 increase in N-type in spring, and S-type persistence decreases in all seasons (Figs 2 and 3d). The
365 AOGCMs showing the largest change in A-type persistence during summer are CNRM-CM5, GFDL-
366 CM3 and MIROC5, with a significant increase of 0.061, 0.059 and 0.035 respectively between 1980s
367 and 2080s. For the C-type in autumn, CSIRO-Mk3.6.0, GFDL-CM3 and HadGEM2-ES show a
368 significant decrease in persistence, between 1980s and 2080s, of 0.157, 0.140 and 0.098 respectively.
369 During winter, for the W-type, the AOGCMs showing the largest change, between the same 1980s and
370 2080s periods, are MRI-CGCM3, CanESM2 and CSIRO-Mk3.6.0 with a significant increase in
371 persistence of 0.367, 0.334 and 0.092 respectively.

372

373 Analysis of RCP4.5 output shows similar, though less marked, results when compared to RCP8.5 (S2
374 Fig). Under the lower emission scenario, we find that most AOGCMs project persistence that falls
375 outside the 95% confidence intervals of the 1980s. A-type MMEM persistence in summer is expected
376 to slightly increase, in particular during the 2080s (Figs S1a-S2a), C-type in autumn may decrease
377 (Figs S1b-S2b), W-type during winter is projected to remain stable across the three future periods (Figs
378 S1c-S2c) and S-type persistence in spring decreases by 2100 (Figs S1d-S2d). Other weather types
379 changes in persistence are found for C-type in summer and A-type in autumn which are set to decrease
380 and a marked increase in E-type during winter; the latter are not in agreement with RCP8.5 (S1 Fig).

381



382

383 **Fig 3. Persistence of selected LWTs and seasons for individual AOGCMs under RCP8.5.** (a) A-type
 384 (summer), (b) C-type (autumn), (c) W-type (winter) and (d) S-type (spring) in the 1980s compared with the
 385 2020s, 2050s and 2080s under RCP8.5. Persistence is shown for individual AOGCMs alongside the MMEM,
 386 20CR, NCEP and Lamb’s catalogue. Asterisks (*) show model runs with persistence outside the 95%
 387 confidence intervals of the boot-strapped (n=1,000) estimates for the 1980s, shown here as black T-bars.

388

389

390 3.3 Frequency of weather patterns (MMEM)

391 Projected frequency trends for selected weather types and seasons under RCP8.5 (2006-2100) are
 392 shown in Fig 4. Summer A- and winter W-type frequencies are expected to rise significantly ($p < 0.01$,
 393 S3 Table) by 0.8 and 0.2 days per decade respectively over the period 2006-2100. Conversely, C- and
 394 S-type frequencies decrease significantly ($p < 0.01$, S3 Table) in autumn and spring respectively. No
 395 significant trends are found for C-type frequency during winter. Sen’s slopes for the MMEM with their
 396 statistical significance are given in S3 Table for each weather type, season and RCP. We also computed
 397 the Sen’s slopes for A-type in each individual AOGCM during summer (RCP8.5, not shown here) to
 398 check whether the increase in A-type was solely due to a few models showing a large increase in this
 399 weather type. We found that all models within the MME show a positive increase in A-type frequency,

400 with 7 out of 10 AOGCMs showing significance at the 90% level, with no outliers skewing the
401 MMEM. Among other seasons (not shown), a significant decrease in annual frequencies is observed
402 for the C-type during summer ($p < 0.01$) and spring ($p < 0.05$), along with a significant ($p < 0.01$) increase
403 in A-type during spring, which all reflect the changes in persistence (Fig 2a and 2d).

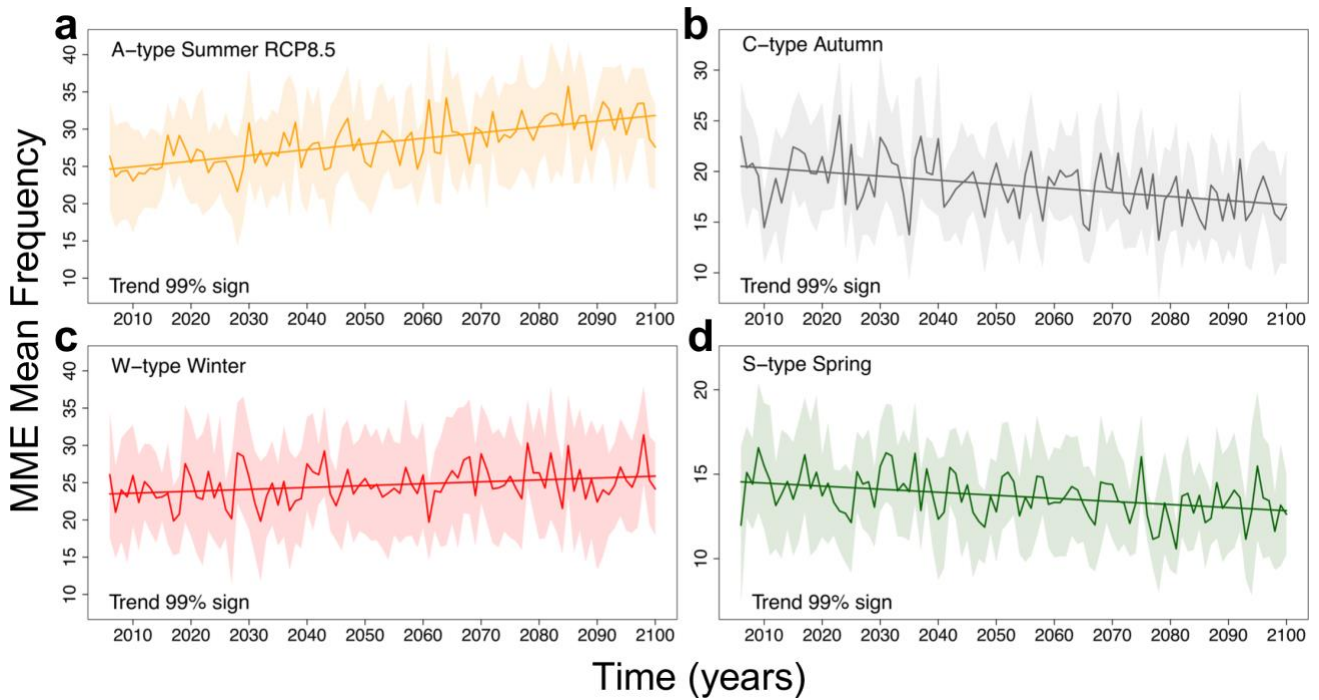
404

405 Projections of MMEM frequencies for the same LWTs and seasons but under RCP4.5 are shown in
406 S3 Fig and S3 Table. Results for RCP4.5 reflect the scenarios of RCP8.5 although the Sen's slopes are
407 less extreme and statistically significant. The A-type frequency is projected to increase significantly
408 ($p < 0.01$, S3a Fig and S3 Table) during summer, C-type in autumn is set to decrease ($p < 0.05$, S3b Fig),
409 W-type frequency in winter shows no significant trend (S3c Fig), and the S-type during spring
410 decreases significantly ($p < 0.05$, S3d Fig). As per RCP8.5, we also observe (not shown) a significant
411 decrease in C-type frequencies during summer ($p < 0.01$) and spring ($p < 0.05$) and an increase in the A-
412 type during spring ($p < 0.05$), matching the relative changes in persistence (Figs S1a and S1d).

413

414

415



416

417 **Fig 4. Projected annual frequencies for selected LWTs and seasons under RCP8.5.** Frequencies are shown
 418 as MMEM for (a) summer anticyclonic A, (b) autumn cyclonic C, (c) winter westerly W and (d) spring southerly
 419 S LWTs under RCP8.5 (2006-2100). Trends are statistically significant at the 1% level (p -value <0.01 , modified
 420 Mann-Kendall test). Shaded areas represent the 95% confidence intervals of the MMEM. The trend lines refer
 421 to the Sen's slopes calculated with the modified Mann-Kendall test.

422

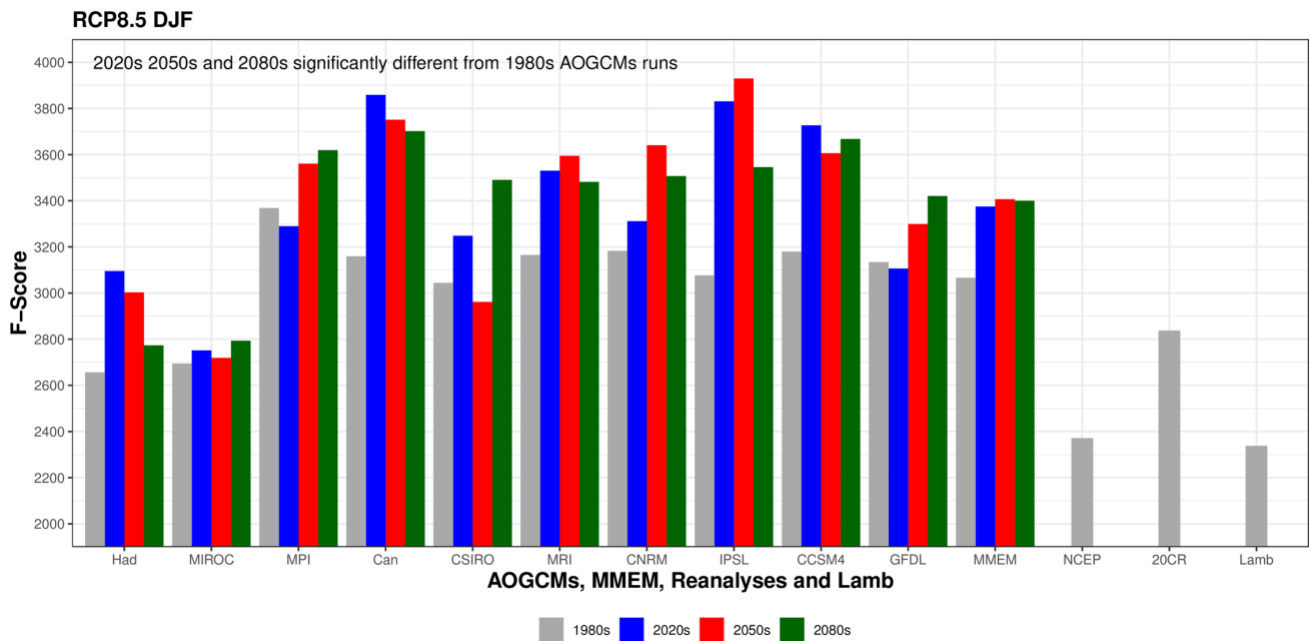
423

424 3.4 Application to future multi-hazards

425 In Fig 5 we extend an earlier analysis [37] based on impactful LWTs found to generate concurrent
 426 flood-wind hazards in GB. Thus, the F-Score for each single AOGCM, MMEM, NCEP, 20CR and
 427 Lamb's subjective datasets and 1980s, 2020s, 2050s and 2080s time periods are shown for winter DJF
 428 weather patterns under RCP8.5. The F-Score is a measure of the severity of future concurrent flood-
 429 wind hazards, such that higher values represent more severe impacts compared to lower ones. Here,
 430 we show that the baseline risk from multiple flood-wind hazards is overestimated by all but two of the
 431 AOGCMs (i.e. HadGEM2-ES and MIROC5) when compared to NCEP, 20CR reanalyses and Lamb's
 432 subjective catalogue for the 1980s. Assuming the same bias holds in the future, AOGCMs likely
 433 overestimate *absolute* future risk from concurrent flood-wind hazards by 2100. Moreover, in a similar

434 way as per Fig 3, there exists a large variability between the AOGCMs, so F-Score results are mixed
435 with some AOGCMs suggesting increased/decreased risk of flood-wind hazards by the end of the 21st
436 century. It is, therefore, always important to use large ensembles to characterise uncertainty in the
437 projections. Lastly, by looking at the MMEM we conclude that, although overestimated by AOGCMs,
438 future risk from concurrent flood-wind hazards could increase by 2100 compared with the 1980s.
439 Among the AOGCMs, those showing the largest F-Score increase between the 1980s and 2080s are
440 CanESM2, CCSM4 and IPSL-CM5A-LR. Results for RCP4.5 are shown in S4 Fig and they agree with
441 what was found for RCP8.5, with large variability amongst AOGCMs and MMEM F-Score even
442 slightly higher than RCP8.5.

443
444
445
446
447
448
449
450



451

452 **Fig 5. F-Score for LWTs associated with concurrent flood-wind hazards during winter DJF.** The F-Score
 453 is shown per each CMIP5 AOGCM, MMEM, NCEP, 20CR and Lamb's subjective catalogue for the 1980s,
 454 2020s, 2050s and 2080s periods. The LWTs used for calculating the F-Score are associated with concurrent
 455 multi-basin floods and wind hazards within Great Britain (GB) [37]. The 1980s MME F-Score were estimated
 456 from the mean of n=1,000 boot-strapped samples and all the future 2020s, 2050s and 2080s periods are
 457 significantly different from these, as the F-Score of the latter fall outside the 95% confidence intervals of the
 458 1980s means. The AOGCMs 1980s confidence intervals bars are not shown for simplicity because they are
 459 vanishingly narrow.

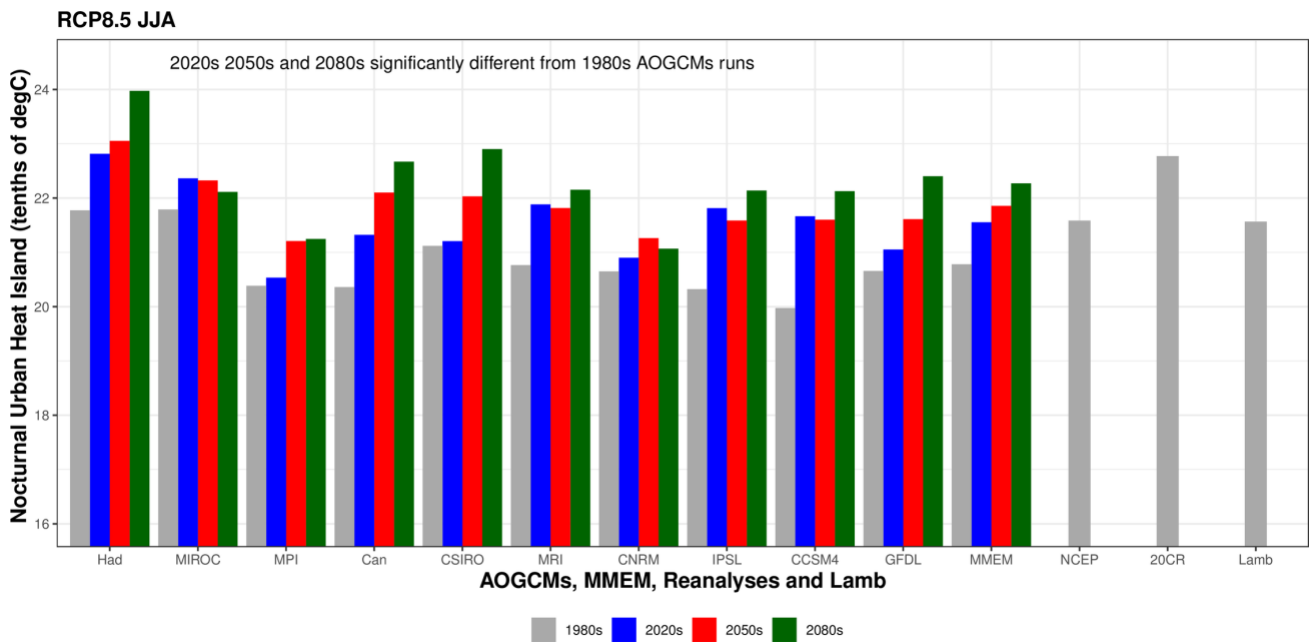
460

461

462 Summer nocturnal UHI temperatures in tenths of °C for London (UK), were estimated for RCP8.5, by
 463 using UHI values obtained in a previous study [40] (Fig 6). Our results show that AOGCMs replicate
 464 nocturnal UHI temperatures, although there is a tendency for underestimation by the majority of
 465 AOGCMs except HadGEM2-ES and MIROC5 which show a good agreement when compared to
 466 NCEP, 20CR and Lamb's subjective catalogue. We also note that there is less variability within the
 467 MME than displayed in Figs 3 and 5. Lastly, almost all the AOGCMs and MMEM show a statistically
 468 significant increase in UHI by the end of 2100, that could eventually translate into an increased multi-
 469 hazard risk from heatwave and poor air quality events associated with persistent A weather types
 470 [40,70–72]. The projected increase in the MMEM UHI between the 1980s and 2080s is 0.15 °C under

471 RCP8.5. The AOGCMs that show the largest increase in nocturnal UHI temperatures between 1980s
 472 and 2080s are CanESM2, HadGEM2-ES and CCSM4 with respectively 0.23, 0.22 and 0.22 °C. Results
 473 for RCP4.5 agree with the RCP8.5 projections although the changes are less marked (S5 Fig).

474
 475



476

477 **Fig 6. As per Fig 5 but for London's nocturnal UHI in tenths of °C during summer JJA.**

478

479

480 **4. Discussion and Conclusions**

481 Greater A-type persistence and frequency during summer likely implies more blocking episodes with
 482 increased risk of poor air quality, drought and heatwaves [1,5,20]. A growing number of studies
 483 propose physical mechanisms that link AA [15] to more persistent weather patterns, which in turn
 484 enhance the likelihood of extreme weather events in the northern hemisphere mid-latitudes. The AA
 485 affects the polar jet stream by making Rossby waves more meridional (or wavier) and by weakening
 486 its flow. A wavier and weaker jet stream in summer favours more persistent extreme weather and it is
 487 also thought to extend ridges northward, enhancing such effects [1–3,17,20–22].

488

489 Our results support earlier analysis [49], and are consistent with the proposed mechanisms linking
490 *observed* AA with mid-latitude weather extremes. On the other hand, AA is expected to have limited
491 effect on simulated CMIP5 blocking over Eurasia under RCP8.5 in the second half of the 21st century
492 [73]. Other work also shows an overall decrease in CMIP5 blocking events over the BI in winter DJF
493 and summer JJA, during 2061-2090 (RCP8.5) [51]. Our findings for anticyclonic weather appear to
494 contradict this. Although A-type persistence and frequency are not exactly the same as blocking, we
495 would expect the studies to agree as both mechanisms involve high pressure weather patterns. The
496 only common denominator between our findings and the studies on blocking [51,73] seems to be the
497 underestimation of A-type/blocking events by CMIP5 models. Further research is needed to reconcile
498 these apparently contradictory findings. Possible explanations are that results depend on the exact
499 spatial domain and/or suite of AOGCMs analysed in each MME, as well as on the methodology used
500 to define A-type days and blocking events.

501

502 Less persistent C-types in autumn suggests lower likelihood of heavy rainfall, with reduced recharge
503 of soil moisture and aquifers at the start of the hydrological year favouring winter droughts. Fewer
504 cyclonic days may also translate into less frequent severe gales and flooding episodes [69], as in GB
505 extreme multi-basin flooding events are strongly associated with C-type weather over time windows
506 from 1 to 19 days [37]. Conversely, more frequent zonal airflow (W-type) in winter may counteract
507 some loss of precipitation from the C-type, especially across higher elevation regions of the north and
508 west BI where there is strong orographic enhancement [74]. Such changes may be attributed to AA,
509 however, the physical mechanisms linking AA to changes in northern hemisphere mid-latitude
510 circulation currently remains an open question.

511

512 From our analyses it is also possible to infer future changes with respect to multi-hazards [28,30],
513 through the F-Score and nocturnal UHI temperatures. Recent analyses show that in GB nearly
514 concurrent multi-basin flooding and extreme wind events are driven by selected LWTs mainly
515 associated with C- and W-types [37]. These multi-hazard events can generate significant economic
516 losses, hence projections of such events may help in evaluating future risks and in improving resilience.
517 We show that during winter DJF the AOGCMs overestimate the F-Score when compared to NCEP,
518 20CR reanalyses and Lamb's subjective dataset. Even so, by the end of 2100 the MMEM shows a
519 statistically significant increase in the F-Score compared with the 1980s within those same models,
520 suggesting that the risk of concurrent flood-wind impacts may become more severe in a warmer world.

521

522 Nocturnal UHI temperatures in London modelled by AOGCMs agree with NCEP, 20CR and Lamb's
523 subjective datasets, although they are slightly underestimated for the 1980s. Nocturnal UHI severity
524 is expected to increase by 2100 under RCP8.5 (MMEM). Our results confirm an increasing trend of
525 ~ 0.3 °C in nocturnal UHI in London found in an earlier study over the observational period 1950-2006
526 [40]. Our findings are also in line with the UK Climate Projections Science Report 2009 [75] which
527 suggests that intense UHI events are highly correlated with A-type weather patterns, and that in
528 London, intense UHI summer events are expected to become more severe in the future [76]. However,
529 further analysis of projections of UHI is needed with a larger model ensemble to better account for
530 uncertainty. Our present findings, when coupled with a significant increase in persistence and
531 frequency of A-type weather pattern, suggests a combined increased risk of heatwaves and poor air
532 quality events in London [40,70–72,76] that could negatively impact human health.

533

534 Finally, we have illustrated how changes in the persistence and frequency of weather patterns are
535 useful diagnostics of climate model realism and can translate into regional to local weather and climate
536 risks scenarios, which could be helpful for developing narratives for decision-makers. However,

537 caution needs to be taken when qualitatively converting synoptic weather pattern changes into local
538 variability because AOGCM skill in reproducing climatic variables at local scales varies significantly
539 and is not always consistent with observations. This is particularly true for precipitation where, for
540 example, pressure fields alone are not able to provide reliable local projections [27].

541

542 With the UK Climate Projections 2018 now partly released and planning underway for the third UK
543 Climate Change Risk Assessment, weather pattern analysis could help to both evaluate the new
544 projections and offer ways of explaining changes that are intelligible to a range of user communities.
545 Similar links to persistence could be made in other regions with established weather pattern typologies,
546 such as the *Grosswetterlagen* for Europe [77], hydrologically important weather types in the
547 contiguous United States [78] and Spatial Synoptic Classification for North America [79].

548

549

550

551

552

553

554

555

556

557

558

559

560

561

562 **References**

- 563 [1] Coumou D, Di Capua G, Vavrus S, Wang L, Wang S. The influence of Arctic amplification
564 on mid-latitude summer circulation. *Nat Commun* 2018;9:2959. doi:10.1038/s41467-018-
565 05256-8.
- 566 [2] Francis J, Skific N. Evidence linking rapid Arctic warming to mid-latitude weather patterns.
567 *Philos Trans R Soc London A Math Phys Eng Sci* 2015;373. doi:10.1098/rsta.2014.0170.
- 568 [3] Francis JA, Vavrus SJ. Evidence linking Arctic amplification to extreme weather in mid-
569 latitudes. *Geophys Res Lett* 2012;39. doi:10.1029/2012GL051000.
- 570 [4] Francis JA, Vavrus SJ. Evidence for a wavier jet stream in response to rapid Arctic warming.
571 *Environ Res Lett* 2015;10:14005.
- 572 [5] Munich Re. Natural catastrophes 2014: Analyses, assessments, positions. 2015.
- 573 [6] Munich Re. NatCatSERVICE - Natural catastrophes in 2018. 2019.
- 574 [7] Stott PA, Stone DA, Allen MR. Human contribution to the European heatwave of 2003.
575 *Nature* 2004;432:610–4. doi:10.1038/nature03089.
- 576 [8] Barriopedro D, Fischer EM, Luterbacher J, Trigo RM, García-Herrera R. The Hot Summer of
577 2010: Redrawing the Temperature Record Map of Europe. *Science* (80-) 2011;332:220 LP-
578 224. doi:10.1126/science.1201224.
- 579 [9] Bastos A, Gouveia CM, Trigo RM, Running SW. Analysing the spatio-temporal impacts of
580 the 2003 and 2010 extreme heatwaves on plant productivity in Europe. *Biogeosciences*
581 2014;11:3421–35. doi:10.5194/bg-11-3421-2014.
- 582 [10] Le Tertre A, Lefranc A, Eilstein D, Declercq C, Medina S, Blanchard M, et al. Impact of the
583 2003 Heatwave on All-Cause Mortality in 9 French Cities. *Epidemiology* 2006;17:75–9.
- 584 [11] Sun Y, Zhang X, Zwiers FW, Song L, Wan H, Hu T, et al. Rapid increase in the risk of
585 extreme summer heat in Eastern China. *Nat Clim Chang* 2014;4:1082.
- 586 [12] Muchan K, Lewis M, Hannaford J, Parry S. The winter storms of 2013/2014 in the UK:

- 587 hydrological responses and impacts. *Weather* 2015;70:55–61. doi:10.1002/wea.2469.
- 588 [13] Kendon M, McCarthy M. The UK's wet and stormy winter of 2013/2014. *Weather*
589 2015;70:40–7. doi:10.1002/wea.2465.
- 590 [14] Matthews T, Murphy C, Wilby RL, Harrigan S. Stormiest winter on record for Ireland and
591 UK. *Nat Publ Gr* 2014;4:738–40. doi:10.1038/nclimate2336.
- 592 [15] Screen JA, Simmonds I. The central role of diminishing sea ice in recent Arctic temperature
593 amplification. *Nature* 2010;464:1334.
- 594 [16] Cohen J, Pfeiffer K, Francis JA. Warm Arctic episodes linked with increased frequency of
595 extreme winter weather in the United States. *Nat Commun* 2018;9:869. doi:10.1038/s41467-
596 018-02992-9.
- 597 [17] Cohen J, Screen JA, Furtado JC, Barlow M, Whittleston D, Coumou D, et al. Recent Arctic
598 amplification and extreme mid-latitude weather. *Nat Geosci* 2014;7:627.
- 599 [18] Hanna E, Hall RJ, Overland JE. Can Arctic warming influence UK extreme weather? *Weather*
600 2017;72:346–52. doi:10.1002/wea.2981.
- 601 [19] Screen JA, Simmonds I. Exploring links between Arctic amplification and mid-latitude
602 weather. *Geophys Res Lett* 2013;40:959–64. doi:10.1002/grl.50174.
- 603 [20] Tang Q, Zhang X, Francis JA. Extreme summer weather in northern mid-latitudes linked to a
604 vanishing cryosphere. *Nat Clim Chang* 2013;4:45.
- 605 [21] Francis JA, Vavrus SJ, Cohen J. Amplified Arctic warming and mid-latitude weather: new
606 perspectives on emerging connections. *Wiley Interdiscip Rev Clim Chang* 2017;8:e474.
607 doi:10.1002/wcc.474.
- 608 [22] Francis JA. Why Are Arctic Linkages to Extreme Weather Still up in the Air? *Bull Am*
609 *Meteorol Soc* 2017;98:2551–7. doi:10.1175/BAMS-D-17-0006.1.
- 610 [23] Di Capua G, Coumou D. Changes in meandering of the Northern Hemisphere circulation.
611 *Environ Res Lett* 2016;11:94028.

- 612 [24] Franzke CLE. Persistent regimes and extreme events of the North Atlantic atmospheric
613 circulation. *Philos Trans R Soc London A Math Phys Eng Sci* 2013;371.
614 doi:10.1098/rsta.2011.0471.
- 615 [25] Hannachi A, Straus DM, Franzke CLE, Corti S, Woollings T. Low-frequency nonlinearity and
616 regime behavior in the Northern Hemisphere extratropical atmosphere. *Rev Geophys*
617 2017;55:199–234. doi:10.1002/2015RG000509.
- 618 [26] Sillmann J, Thorarinsdottir T, Keenlyside N, Schaller N, Alexander L V, Hegerl G, et al.
619 Understanding, modeling and predicting weather and climate extremes: Challenges and
620 opportunities. *Weather Clim Extrem* 2017;18:65–74.
621 doi:https://doi.org/10.1016/j.wace.2017.10.003.
- 622 [27] Murawski A, Bürger G, Vorogushyn S, Merz B. Can local climate variability be explained by
623 weather patterns? A multi-station evaluation for the Rhine basin. *Hydrol Earth Syst Sci*
624 2016;20:4283–306. doi:10.5194/hess-20-4283-2016.
- 625 [28] Zscheischler J, Westra S, van den Hurk BJJM, Seneviratne SI, Ward PJ, Pitman A, et al.
626 Future climate risk from compound events. *Nat Clim Chang* 2018;8:469–77.
627 doi:10.1038/s41558-018-0156-3.
- 628 [29] AghaKouchak A, Huning LS, Mazdidasni O, Mallakpour I, Chiang F, Sadegh M, et al. How
629 do natural hazards cascade to cause disasters? *Nature* 2018;561:458–60. doi:10.1038/d41586-
630 018-06783-6.
- 631 [30] Gill JC, Malamud BD. Reviewing and visualizing the interactions of natural hazards. *Rev*
632 *Geophys* 2014;52:680–722. doi:10.1002/2013RG000445.
- 633 [31] Kappes MS, Keiler M, von Elverfeldt K, Glade T. Challenges of analyzing multi-hazard risk:
634 a review. *Nat Hazards* 2012;64:1925–58. doi:10.1007/s11069-012-0294-2.
- 635 [32] Terzi S, Torresan S, Schneiderbauer S, Critto A, Zebisch M, Marcomini A. Multi-risk
636 assessment in mountain regions: A review of modelling approaches for climate change

- 637 adaptation. *J Environ Manage* 2019;232:759–71.
638 doi:<https://doi.org/10.1016/j.jenvman.2018.11.100>.
- 639 [33] Forzieri G, Feyen L, Russo S, Vousdoukas M, Alfieri L, Outten S, et al. Multi-hazard
640 assessment in Europe under climate change. *Clim Change* 2016;137:105–19.
641 doi:10.1007/s10584-016-1661-x.
- 642 [34] Gallina V, Torresan S, Critto A, Sperotto A, Glade T, Marcomini A. A review of multi-risk
643 methodologies for natural hazards: Consequences and challenges for a climate change impact
644 assessment. *J Environ Manage* 2016;168:123–32.
645 doi:<http://dx.doi.org/10.1016/j.jenvman.2015.11.011>.
- 646 [35] UNISDR. Sendai Framework for Disaster Risk Reduction 2015 - 2030. Third World Conf
647 Disaster Risk Reduction, Sendai, Japan, 14-18 March 2015 2015:1–25.
648 doi:A/CONF.224/CRP.1.
- 649 [36] Kargel JS, Leonard GJ, Shugar DH, Haritashya UK, Bevington A, Fielding EJ, et al.
650 Geomorphic and geologic controls of geohazards induced by Nepal’s 2015 Gorkha
651 earthquake. *Science* (80-) 2016;351:aac8353. doi:10.1126/science.aac8353.
- 652 [37] De Luca P, Hillier JK, Wilby RL, Quinn NW, Harrigan S. Extreme multi-basin flooding
653 linked with extra-tropical cyclones. *Environ Res Lett* 2017;12:114009.
- 654 [38] Ward PJ, Couasnon A, Eilander D, Haigh ID, Hendry A, Muis S, et al. Dependence between
655 high sea-level and high river discharge increases flood hazard in global deltas and estuaries.
656 *Environ Res Lett* 2018;13:84012. doi:10.1088/1748-9326/aad400.
- 657 [39] Collet L, Harrigan S, Prudhomme C, Formetta G, Beevers L. Future hot-spots for hydro-
658 hazards in Great Britain: a probabilistic assessment. *Hydrol Earth Syst Sci* 2018;22:5387–401.
659 doi:10.5194/hess-22-5387-2018.
- 660 [40] Wilby RL, Jones PD, Lister DH. Decadal variations in the nocturnal heat island of London.
661 *Weather* 2011;66:59–64. doi:10.1002/wea.679.

- 662 [41] Merz B, Aerts J, Arnbjerg-Nielsen K, Baldi M, Becker A, Bichet A, et al. Floods and climate:
663 emerging perspectives for flood risk assessment and management. *Nat Hazards Earth Syst Sci*
664 2014;14:1921–42. doi:10.5194/nhess-14-1921-2014.
- 665 [42] Conticello F, Cioffi F, Merz B, Lall U. An event synchronization method to link heavy rainfall
666 events and large-scale atmospheric circulation features. *Int J Climatol* 2018;38:1421–37.
667 doi:10.1002/joc.5255.
- 668 [43] Farnham DJ, Doss-Gollin J, Lall U. Regional Extreme Precipitation Events: Robust Inference
669 From Credibly Simulated GCM Variables. *Water Resour Res* 2018;54:3809–24.
670 doi:10.1002/2017WR021318.
- 671 [44] Murawski A, Vorogushyn S, Bürger G, Gerlitz L, Merz B. Do Changing Weather Types
672 Explain Observed Climatic Trends in the Rhine Basin? An Analysis of Within- and Between-
673 Type Changes. *J Geophys Res Atmos* 2018;123:1562–84. doi:10.1002/2017JD026654.
- 674 [45] Pattison I, Lane SN. The relationship between Lamb weather types and long-term changes in
675 flood frequency, River Eden, UK. *Int J Climatol* 2012;32:1971–89. doi:10.1002/joc.2415.
- 676 [46] Matthews T, Murphy C, Wilby RL, Harrigan S. A cyclone climatology of the British-Irish
677 Isles 1871–2012. *Int J Climatol* 2016;36:1299–312. doi:10.1002/joc.4425.
- 678 [47] Wilby RL, Wigley TML. Downscaling general circulation model output: a review of methods
679 and limitations. *Prog Phys Geogr Earth Environ* 1997;21:530–48.
680 doi:10.1177/030913339702100403.
- 681 [48] Xu H, Corte-Real J, Qian B. Developing daily precipitation scenarios for climate change
682 impact studies in the Guadiana and the Tejo basins. *Hydrol Earth Syst Sci* 2007;11:1161–73.
683 doi:10.5194/hess-11-1161-2007.
- 684 [49] Otero N, Sillmann J, Butler T. Assessment of an extended version of the Jenkinson–Collison
685 classification on CMIP5 models over Europe. *Clim Dyn* 2018;50:1559–79.
686 doi:10.1007/s00382-017-3705-y.

- 687 [50] Stryhal J, Huth R. Trends in winter circulation over the British Isles and central Europe in
688 twenty-first century projections by 25 CMIP5 GCMs. *Clim Dyn* 2018;0:0.
689 doi:10.1007/s00382-018-4178-3.
- 690 [51] Woollings T, Barriopedro D, Methven J, Son S-W, Martius O, Harvey B, et al. Blocking and
691 its Response to Climate Change. *Curr Clim Chang Reports* 2018. doi:10.1007/s40641-018-
692 0108-z.
- 693 [52] Taylor KE, Stouffer RJ, Meehl GA. An Overview of CMIP5 and the Experiment Design. *Bull*
694 *Am Meteorol Soc* 2011;93:485–98. doi:10.1175/BAMS-D-11-00094.1.
- 695 [53] Lamb HH. British Isles Weather types and a register of daily sequence of circulation patterns,
696 1861-1971. *Geophysical Memoir* 116, London, HMSO; 1972.
- 697 [54] Jones PD, Hulme M, Briffa KR. A comparison of Lamb circulation types with an objective
698 classification scheme. *Int J Climatol* 1993;13:655–63. doi:10.1002/joc.3370130606.
- 699 [55] Jones PD, Harpham C, Briffa KR. Lamb weather types derived from reanalysis products. *Int J*
700 *Climatol* 2013;33:1129–39. doi:10.1002/joc.3498.
- 701 [56] Jenkinson AF, Collison FP. An Initial Climatology of Gales over the North Sea. *Synoptic*
702 *Climatology Branch Memorandum No. 62*, Meteorological Office, Bracknell; 1977.
- 703 [57] Compo GP, Whitaker JS, Sardeshmukh PD, Matsui N, Allan RJ, Yin X, et al. The Twentieth
704 Century Reanalysis Project. *Q J R Meteorol Soc* 2011;137:1–28. doi:10.1002/qj.776.
- 705 [58] Kalnay E, Kanamitsu M, Kistler R, Collins W, Deaven D, Gandin L, et al. The NCEP/NCAR
706 40-Year Reanalysis Project. *Bull Am Meteorol Soc* 1996;77:437–71. doi:10.1175/1520-
707 0477(1996)077<0437:TNYRP>2.0.CO;2.
- 708 [59] Hulme M, Barrow E. *Climate of the British Isles: present, past and future*. London: Routledge;
709 1997.
- 710 [60] Lamb HH. Types and spells of weather around the year in the British Isles : Annual trends,
711 seasonal structure of the year, singularities. *Q J R Meteorol Soc* 1950;76:393–429.

- 712 doi:10.1002/qj.49707633005.
- 713 [61] Hulme M, Briffa KR, Jones PD, Senior CA. Validation of GCM control simulations using
714 indices of daily airflow types over the British Isles. *Clim Dyn* 1993;9:95–105.
715 doi:10.1007/BF00210012.
- 716 [62] Jones PD, Osborn TJ, Harpham C, Briffa KR. The development of Lamb weather types: from
717 subjective analysis of weather charts to objective approaches using reanalyses. *Weather*
718 2014;69:128–32. doi:10.1002/wea.2255.
- 719 [63] Wilby RL. Stochastic weather type simulation for regional climate change impact assessment.
720 *Water Resour Res* 1994;30:3395–403. doi:10.1029/94WR01840.
- 721 [64] Gagniuc PA. *Markov Chains: From Theory to Implementation and Experimentation*. USA,
722 NJ: John Wiley & Sons; 2017. doi:10.1002/9781119387596.
- 723 [65] Spedicato GA. Discrete Time Markov Chains with R. *R J* 2017;9:84–104.
- 724 [66] Mann HB, Whitney DR. On a Test of Whether one of Two Random Variables is
725 Stochastically Larger than the Other. *Ann Math Stat* 1947;18:50–60.
726 doi:10.1214/aoms/1177730491.
- 727 [67] Hamed KH, Ramachandra Rao A. A modified Mann-Kendall trend test for autocorrelated
728 data. *J Hydrol* 1998;204:182–96. doi:https://doi.org/10.1016/S0022-1694(97)00125-X.
- 729 [68] Sen PK. Estimates of the Regression Coefficient Based on Kendall’s Tau. *J Am Stat Assoc*
730 1968;63:1379–89. doi:10.1080/01621459.1968.10480934.
- 731 [69] Wilby RL, Quinn NW. Reconstructing multi-decadal variations in fluvial flood risk using
732 atmospheric circulation patterns. *J Hydrol* 2013;487:109–21.
733 doi:10.1016/j.jhydrol.2013.02.038.
- 734 [70] O’Hare GPP, Wilby RL. A Review of Ozone Pollution in the United Kingdom and Ireland
735 with an Analysis Using Lamb Weather Types. *Geogr J* 1995;161:1–20. doi:10.2307/3059923.
- 736 [71] Pope RJ, Savage NH, Chipperfield MP, Arnold SR, Osborn TJ. The influence of synoptic

737 weather regimes on UK air quality: analysis of satellite column NO₂. *Atmos Sci Lett*
738 2014;15:211–7. doi:10.1002/asl2.492.

739 [72] Pope RJ, Butt EW, Chipperfield MP, Doherty RM, Fenech S, Schmidt A, et al. The impact of
740 synoptic weather on UK surface ozone and implications for premature mortality. *Environ Res*
741 *Lett* 2016;11. doi:10.1088/1748-9326/11/12/124004.

742 [73] Woollings T, Harvey B, Masato G. Arctic warming, atmospheric blocking and cold European
743 winters in CMIP5 models. *Environ Res Lett* 2014;9:14002.

744 [74] Burt TP, Howden NJK. North Atlantic Oscillation amplifies orographic precipitation and river
745 flow in upland Britain. *Water Resour Res* 2013;49:3504–15. doi:10.1002/wrcr.20297.

746 [75] Murphy JM, Sexton DMH, Jenkins GJ, Boorman PM, Booth BBB, Brown CC, et al. UK
747 Climate Projections Science Report: Climate change projections. Exeter: 2009.

748 [76] Wilby RL. Constructing Climate Change Scenarios of Urban Heat Island Intensity and Air
749 Quality. *Environ Plan B Plan Des* 2008;35:902–19. doi:10.1068/b33066t.

750 [77] Hess P, Brezowsky H. Katalog der Großwetterlagen Europas. Berichte des Deutschen
751 Wetterdienstes in der US-Zone 33. Deutscher Wetterdienst in d. US-Zone: Bad Kissingen.;
752 1952.

753 [78] Prein AF, Bukovsky MS, Mearns LO, Bruyère CL, Done JM. Simulating North American
754 Weather Types With Regional Climate Models. *Front Environ Sci* 2019;7:36.

755 [79] Kalkstein LS, Nichols MC, Barthel CD, Greene JS. A new spatial synoptic classification:
756 application to air-mass analysis. *Int J Climatol* 1996;16:983–1004. doi:10.1002/(SICI)1097-
757 0088(199609)16:9<983::AID-JOC61>3.0.CO;2-N.

758

759

760